Electronic Supplementary Information

Oxygen Vacancy Content Drives Self-Reduction and Anti-Thermal Quenching

Yuxing Bai,[a] Shaojun Sun,[a] Liwei Wu,[a, b] Tiangui Hu,[c] Lirong Zheng,[d] Li Wu,*[a] Yongfa Kong,[a] Yi Zhang,[d] and Jingjun Xu [a]

[a]Key Laboratory of Weak-Light Nonlinear Photonics, Ministry of Education, School of Physics, Nankai University, Tianjin 300071, China. E-mail: *lwu@nankai.edu.cn
[b]College of Science, Civil Aviation University of China, Tianjin 300300, China
[c]State Key Laboratory of Superlattices and Microstructures, Institute of Semiconductors, Chinese Academy of Sciences, Beijing 100083, China
[d]Multi-Discipline Research Center, Institute of High Energy Physics, Chinese Academy of Sciences, Beijing 100049, China
[e]Institute of Photo-electronic Thin Film Devices and Technology, Nankai University, Tianjin 300071, China

Experimental section

Materials and synthesis: The as-prepared samples $LiZn_{1-x}PO_4:xMn^{2+}$ ($0 \leq x \leq 0.16$) were synthesized via a high-temperature solid-state method in an ambient atmosphere. The compound $LiZnPO_4:Mn^{2+}$ were synthesized starting from Li_2CO_3 (99.99, excess of 3%), ZnO (99.99%), $NH_4H_2PO_4$ (99.99%) and MnO_2 (99.99%). All of them were weighted according to the molar ratio and thoroughly mixed in an agate mortar. Then the processed mixtures were pre-heated at 600 °C for 12 h in a crucible to decompose the carbonates and eliminate water. After cooling to room temperature, the pre-sintered samples were reground and sintered at 990 °C for 24 h. Finally, the sintered products were well ground into powders to use in subsequent performance characterizations. For comparison, the mixed materials (Li_2CO_3, ZnO, $NH_4H_2PO_4$ and MnO_2 (99.99%)) were transferred into a tube furnace and calcinated at 890 °C under a reducing atmosphere of H_2 (15%) +Ar (85%). After 6 h, the $LiZnPO_4:0.14Mn^{2+}$ ($LZPM_{0.14}$-H) sample was obtained.

Characterization: Powder XRD patterns were collected on a D8 ADVANCE diffractometer (X'Pert Pro, PANalytical B.V., Netherlands) operating at 40 kV and 40 mA with Cu Kα radiation (λ = 1.5406 Å). The refinement data for Rietveld analysis were gathered in step-scanning mode over the 2θ range from 10° to 120° at intervals of 0.017°. The photoluminescence (PL) and photoluminescence excitation (PLE) spectra at room temperature were measured using a fluorescence spectrometer (Edinburgh Instruments, FLS920, England) equipped with a 150 w xenon lamp. The fluorescence lifetime of millisecond was obtained using a 100 w μF900 lamp as the light source and a R928P photo-multiplier as the detector. The temperature-dependent luminescence properties were also studied using the same spectrofluorometer with a heating apparatus (Tianjin Orient Koji Co., Ltd, TAP-02). Scanning electron microscopy (SEM, SU8020, HITACHI, Japan) with energy dispersive X-ray spectroscopy (EDS, EMAX, HORIBA) was used to characterize the morphology of the samples. X-ray photoelectron spectroscopy (XPS) were recorded using a Thermo Scientific ESCALAB 250Xi (America) and calibrated to a C 1*s* electron peak at 284.8 eV. X-band (9.844 GHz) EPR spectrum was adopted on a Bruker EMX-6/1 EPR spectrometer. The XAFS spectra were tested via the 1W1B beam line (Beijing Synchrotron Radiation Facility). The diffuse reflectance (DR) information can be known from a UV/Vis/NIR spectrophotometer (Cary5000, America). Inductively Coupled Plasma Optical Emission Spectrometer (ICP-OES) was considered to examine the amounts of all the elements by means of Agilent ICPOES730 (America) with the power of 1.0 KW.

After pre-irradiating with 365 nm UV light for 15 min, 30 min, and 60 min, thermoluminescence (TL) curves of the powder samples were obtained using a thermoluminescence meter (FJ427A1, CNCS, China).

Computational methods: All the DFT calculations were implemented with the Vienna ab initio simulation package (VASP). The electron-ion interactions were determined using the projector augmented wave pseudo-potential method.[1] Li ($1s^2 2s^1$), Zn ($3d^{10}$), P ($3s^2 3p^3$), O ($2s^2 2p^4$) and Mn ($3d^6 4s^1$) electrons were treated as their own valence electrons. To investigate the density of states accurately, the spin-polarized generalized gradient approximation with the Perdew-Burke-Ernzerhof functional was adopted to describe the electronic exchange-correlation potential.[2] The cutoff energy of 400 eV was used for the plane-wave basis set to expand the pseudo valence wave function. A $2 \times 1 \times 1$ supercell was constructed, in which Zn ions were substituted by Mn ions. Moreover, k-point grids for the Brillouin zone were generated with $2 \times 2 \times 1$ and $1 \times 1 \times 1$ G-centered models for the primitive-cell and super-cell, respectively. All the optimization processes were considered to satisfy the convergence criterion when the total energy change was less than 1×10^{-4} eV per step, and the maximum force was less than 5×10^{-2} eV Å^{-1} per atom.

LED fabrication: The w-LED was successfully fabricated through combining commercial red phosphor (Sr, Ca)SiAlN$_3$:Eu^{2+}, blue phosphor BaMgAl$_{10}$O$_{17}$:Eu^{2+}, green phosphor (Sr, Ba)$_2$SiO$_4$:Eu^{2+} and our yellow phosphor LiZnPO$_4$:Mn^{2+} with a UV-LED chip (λ = 370 nm). The phosphors were thoroughly mixed with epoxy resin, and the obtained phosphor-epoxy resin mixture was coated on the LED chips. The photoelectric properties, including the electroluminescent (EL) spectrum, luminous efficacy, CCT, color rendering index (R_a) as well as CIE color coordinates of the LED, were characterized by using a photometry colorimeter & electricity test system equipped with an integrating sphere (HP9000, Hopoo, China).
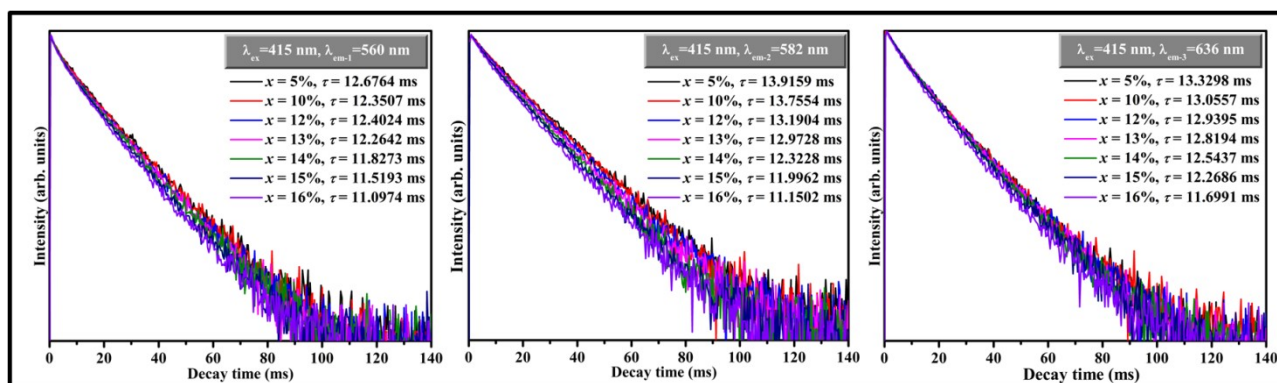

Fig. S1 Decay curves of LiZnPO$_4$:0.14Mn^{2+} excited by NUV light of 415 nm and monitored at different emission wavelengths.
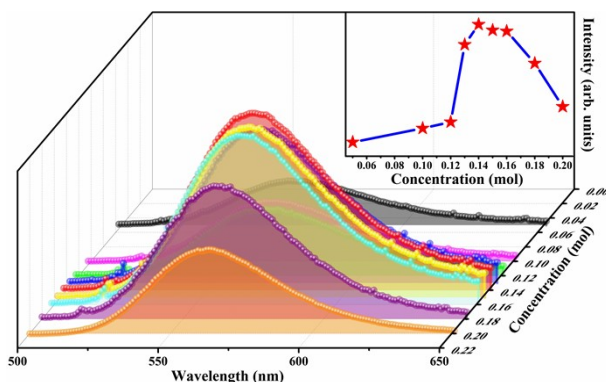

Fig. S2 PL spectra of LiZnPO$_4$:xMn^{2+} ($0 \leq x \leq 0.20$) under the excitation of 415 nm; the inset shows the emission intensity versus Mn^{2+}-doped concentration.

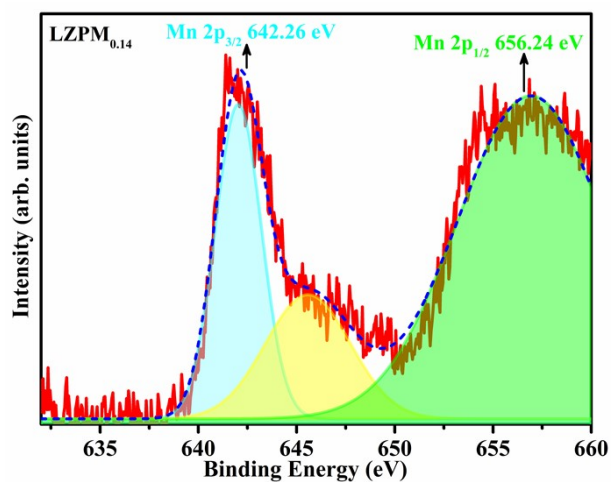Fig. S3 High-resolution XPS spectrum of Mn 2p for LiZnPO$_4$:0.14Mn^{2+}.

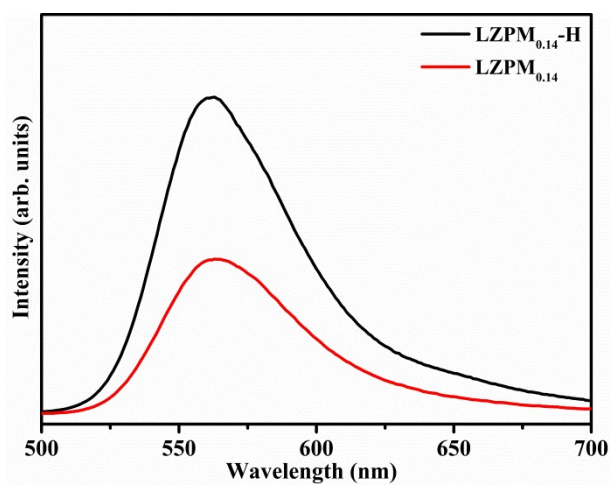Fig. S4 The PL spectra of LiZnPO$_4$:0.14Mn^{2+} calcinated in ambient and reducing atmosphere, respectively.
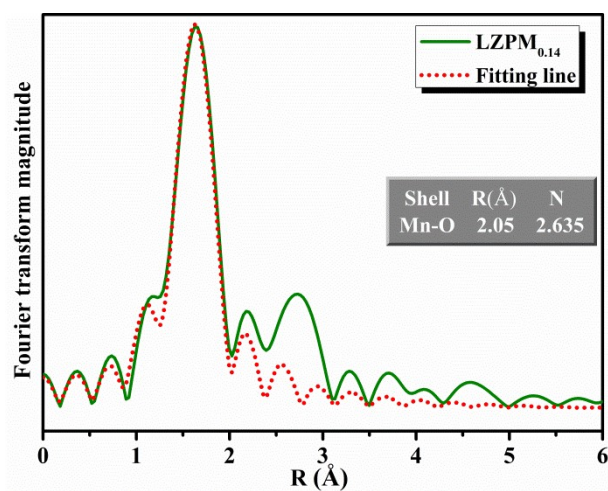

Fig. S5 Fourier transforms of K-edge EXAFS spectra and fitting results of the first neighbor Mn-O coordination of LiZnPO$_4$:0.14Mn^{2+}. The inset shows the calculated structural parameters of Mn-O shell.

In ultraviolet-visible diffuse reflectance spectra (DRS) of host and doped samples, each of peak including the strongest absorption position at 415 nm matches with those in PLE spectra. The optical band gap (E_g) is determined through the following Kubelka-Munk equation:[3]

$$\left[F(R_\infty)h\nu\right]^n = A(h\nu - E_g) \tag{1}$$

where $h\nu$ represents the photon energy, A is the proportional constant and n denotes the feature of direct and indirect transition, respectively. The absorption coefficient $F(R_\infty)$ can be obtained by the formula:

$$F(R_\infty) = (1-R)^2/2R \tag{2}$$

where R stands for the reflection coefficient. The curves of $[F(R_\infty)h\nu]^2$ to $h\nu$ are plotted and E_g is acquired by extrapolating the linear portion of the plot to $[F(R_\infty)h\nu]^2 = 0$. The optical band gaps of LZP and LZPM$_{0.14}$ are calculated to be 5.36 eV and 5.27 eV, respectively.
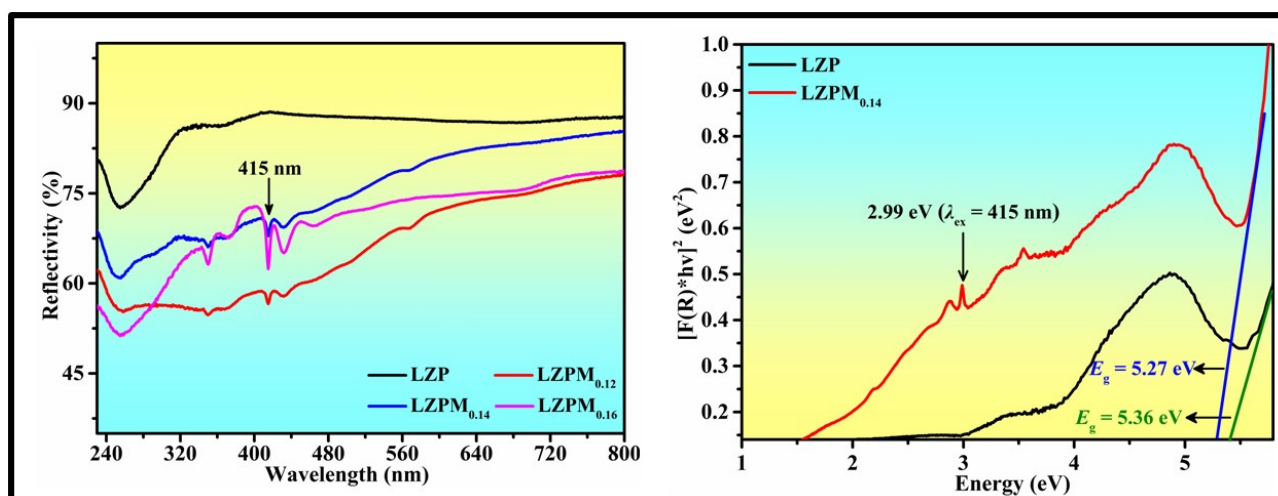

Fig. S6 Ultraviolet-visible diffuse reflectance spectra of LiZnPO$_4$, LiZnPO$_4$:0.12Mn^{2+}, LiZnPO$_4$:0.14Mn^{2+} and LiZnPO$_4$:0.16Mn^{2+}.
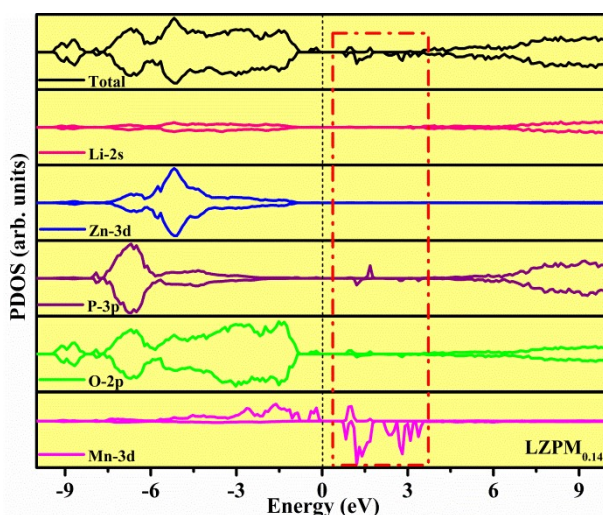

Fig. S7 Total and partial density of states for LiZnPO$_4$:0.14Mn^{2+}.

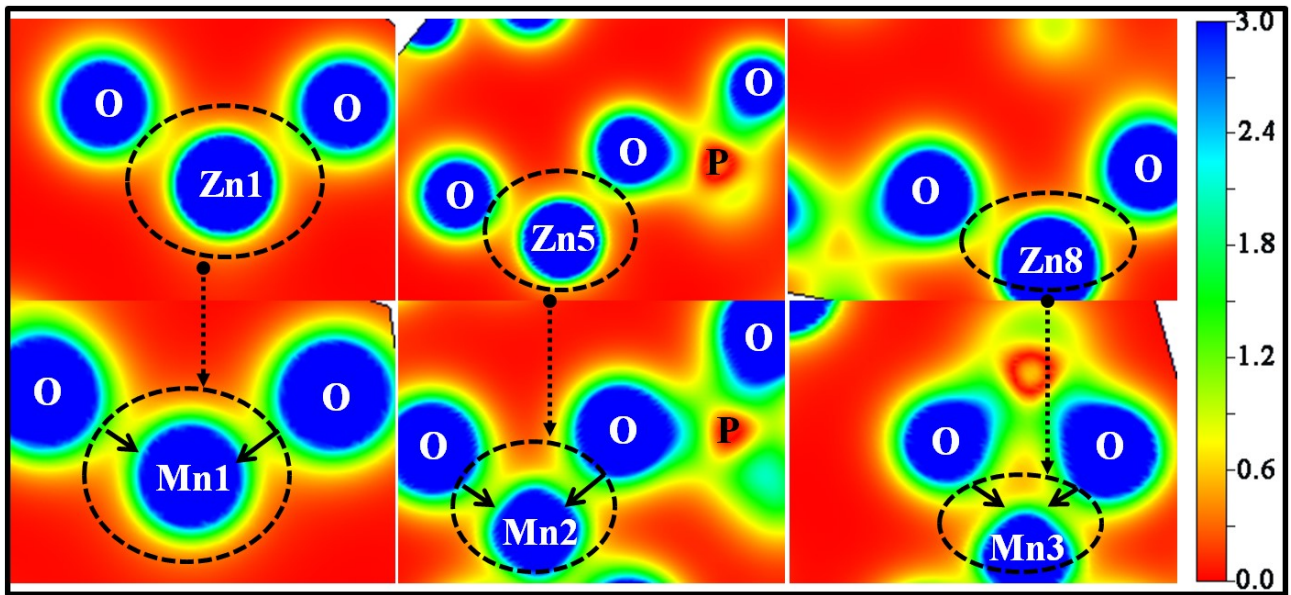Fig. S8 Two-dimensional electron localization function (ELF) maps around Zn/Mn sites for $LiZnPO_4$ and $LiZnPO_4:0.14Mn^{2+}+V_O$.
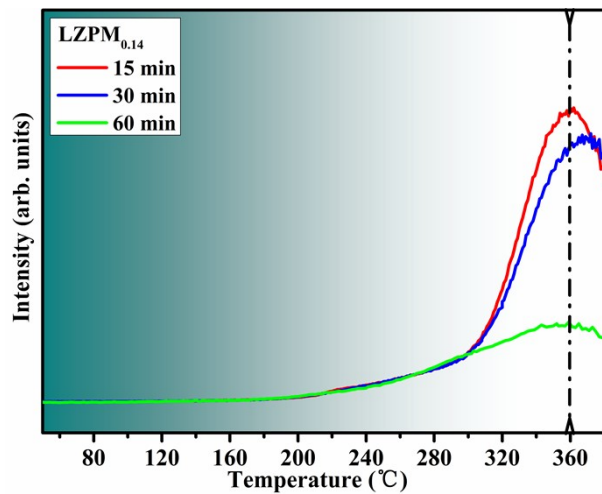
Fig. S9 TL spectrum of $LiZnPO_4:0.14Mn^{2+}$ under different pre-irradiation time.
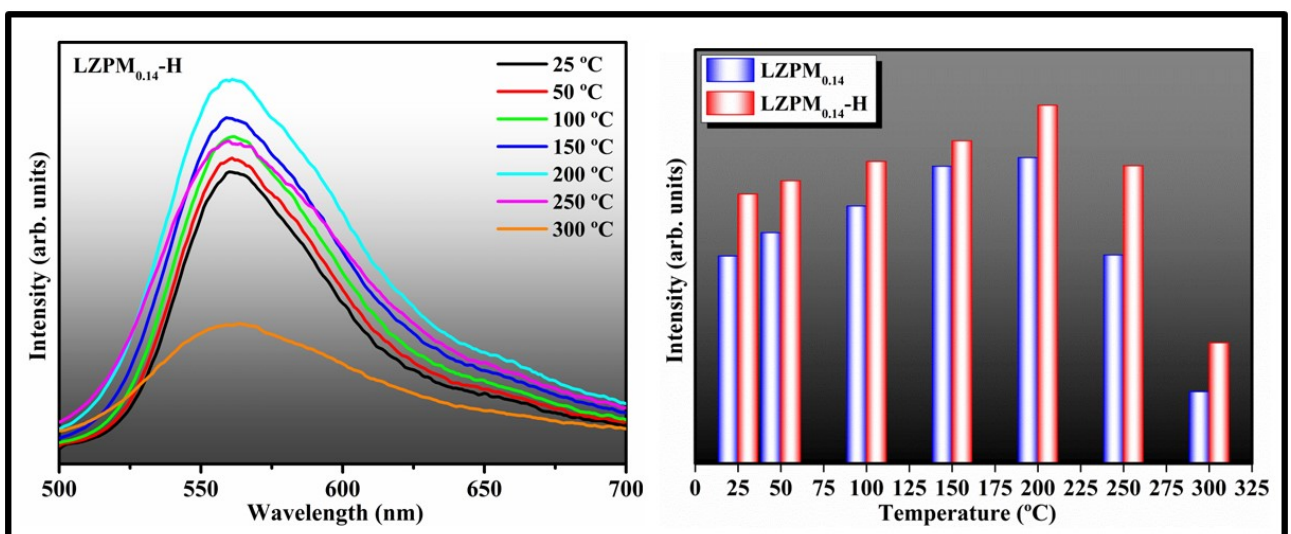
Fig. S10 Temperature-dependent PL spectrum of LiZnPO$_4$:0.14Mn^{2+} synthesized at reducing atmosphere, and the relationship between emission intensity and temperature for the samples synthesized at different environments.

	O1	O2
Energy	530.86	531.36

	O1	O2
Energy	530.94	531.4
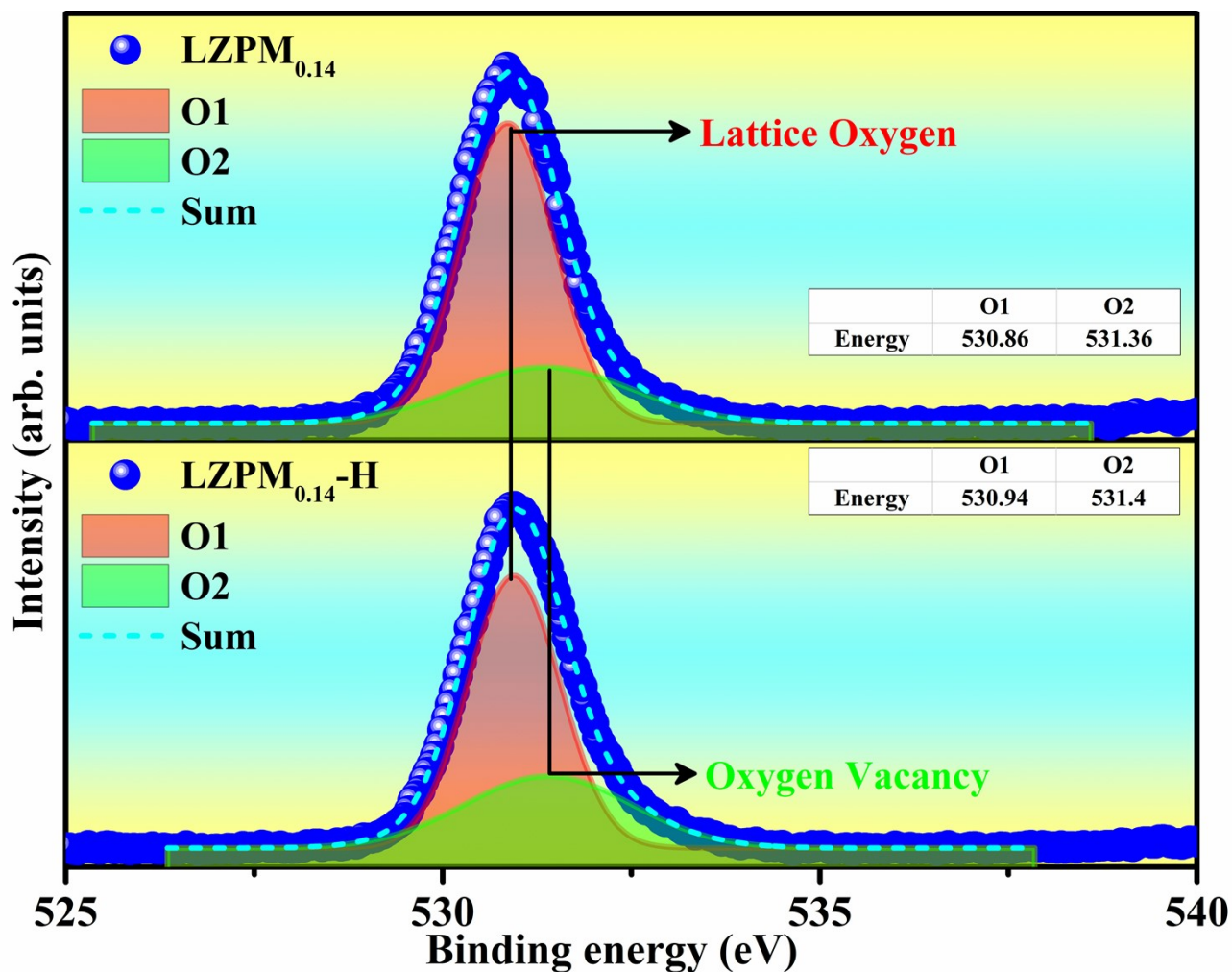
Fig. S11 High-resolution XPS spectra of O 1s for LiZnPO$_4$:0.14Mn^{2+} prepared in air and reducing atmosphere.

Fig. S12 Normalized temperature-dependent PL spectra for LiZnPO$_4$:0.14Mn^{2+}.
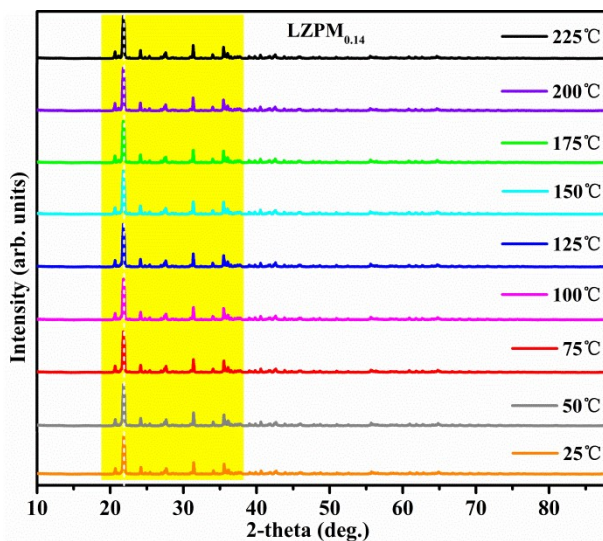
Fig. S13 Temperature-dependent XRD patterns of LiZnPO$_4$:0.14Mn^{2+}.

Table S1 The total Helmholtz free energy when Mn^{2+} ions occupy Zn^{2+} or Li$^+$ sites.

Model	Total energy
Mn$_{Li}$+V$_O$+V$_{Li}$	-676.23
Mn$_{Zn}$+V$_O$	-703.68

Table S2 Lattice parameters and agreement factors for LiZnPO$_4$:0.14Mn^{2+} refined by Rietveld method.
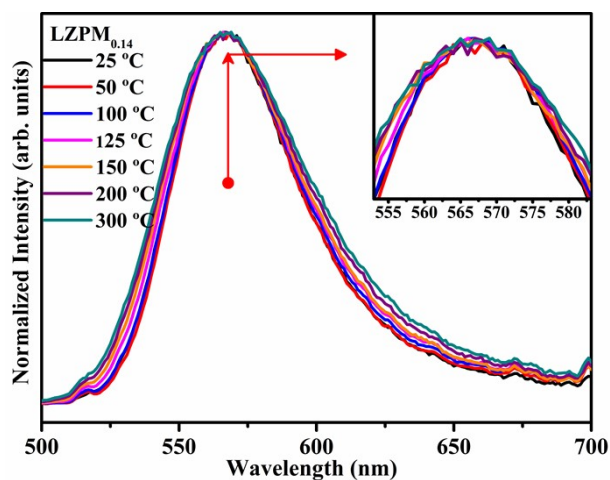
Samples	LiZnPO$_4$:Mn^{2+}
Crystal system	Monoclinic
Space group	*Cc*
a/Å	17.3025(1)
b/ Å	9.7847(1)
c/ Å	17.1392(1)
V/Å^3	2711.43(6)
Z	32
Radiation type	Cu-Kα
Wavelength (Å)	1.5406
Profile range (°2θ)	10-140
Step size (°2θ)	0.017
R$_p$ (%)	7.152
R$_{wp}$ (%)	9.400
R$_{exp}$ (%)	4.509
R$_{Bragg}$ (%)	4.132
GOF	2.085

Table S3 Refined atomic positions and occupancies for LiZnPO$_4$:0.14Mn^{2+}.

Atoms	Wyckoff sites	*x*	*y*	*z*	Occupancy
Zn1	4a	0.9490(12)	-0.28630(10)	0.4639(10)	0.959(13)

Mn1	4a	0.9490(12)	-0.28630(10)	0.4639(10)	**0.041(13)**
Zn2	4a	0.1972(4)	0.9673(6)	0.4658(4)	1.00000
Zn3	4a	-0.08330	-0.1828(3)	-0.036(3)	1.00000
Zn4	4a	0.1649(4)	0.3180(6)	0.2199(4)	1.00000
Zn5	4a	0.9125(5)	0.0578(8)	0.2182(5)	0.964(13)
Mn2	4a	0.9125(5)	0.0578(8)	0.2182(5)	**0.036(13)**
Zn6	4a	0.6308(3)	0.2902(7)	0.2200(4)	1.00000
Zn7	4a	0.1705(4)	0.4262(7)	0.4701(4)	1.00000
Zn8	4a	-0.1160(5)	-0.4659(2)	0.2151(13)	0.940(11)
Mn3	4a	-0.1160(5)	-0.4659(2)	0.2151(13)	**0.060(11)**
Li1	4a	-0.21270	-0.69370	0.10030	1.00000
Li2	4a	-0.17660	-0.21880	0.08800	1.00000
Li3	4a	0.03460	-0.17810	0.33930	1.00000
Li4	4a	0.00300	-0.70980	0.33800	1.00000
Li5	4a	-0.21520	-0.43320	0.33950	1.00000
Li6	4a	-0.24410	0.03920	0.33990	1.00000
Li7	4a	0.04470	0.06360	0.08900	1.00000
Li8	4a	0.06940	-0.46400	0.08620	1.00000
P1	4a	0.8577(8)	0.0647(12)	0.0347(8)	1.00000
P2	4a	0.8802(6)	0.5227(11)	0.0259(7)	1.00000
P3	4a	-0.14930(10)	-0.18810(20)	0.27750(10)	1.00000
P4	4a	-0.17970(10)	-0.71590(20)	0.27560(10)	1.00000
P5	4a	0.13320(10)	-0.28260(20)	0.52690(10)	1.00000
P6	4a	-0.39820(10)	-0.68860(10)	0.02470(10)	1.00000
P7	4a	0.07230(10)	-0.46800(20)	0.27590(10)	1.00000
P8	4a	0.09900(10)	0.06120(20)	0.27770(10)	1.00000
O1	4a	-0.16440	-0.03530	-0.04950	1.00000
O2	4a	-0.22270	0.15440	0.00940	1.00000
O3	4a	-0.13010	-0.02900	0.10480	1.00000
O4	4a	-0.06890	0.15020	0.03840	1.00000
O5	4a	-0.04260	-0.53250	0.01560	1.00000
O6	4a	-0.19640	-0.49870	-0.05180	1.00000
O7	4a	-0.10460	-0.31340	0.04040	1.00000
O8	4a	-0.13660	-0.53420	0.10100	1.00000
O9	4a	-0.15770	-0.27920	0.20100	1.00000
O10	4a	-0.13260	-0.28480	0.35220	1.00000
O11	4a	-0.22850	-0.10350	0.26100	1.00000
O12	4a	-0.07480	-0.09040	0.29450	1.00000
O13	4a	-0.10240	-0.75160	0.35240	1.00000
O14	4a	-0.16540	-0.78120	0.19930	1.00000
O15	4a	-0.25700	-0.77470	0.28750	1.00000
O16	4a	-0.19030	-0.56110	0.26280	1.00000
O17	4a	0.11900	-0.22730	0.60360	1.00000
O18	4a	0.20940	-0.21930	0.51540	1.00000

O19	4a	0.14610	-0.43770	0.53960	1.00000
O20	4a	0.05480	-0.25030	0.45040	1.00000
O21	4a	-0.38390	-0.77710	0.10140	1.00000
O22	4a	-0.32130	-0.60080	0.03900	1.00000
O23	4a	-0.41310	-0.78350	-0.05100	1.00000
O24	4a	-0.47450	-0.59530	0.00950	1.00000
O25	4a	0.05970	-0.31210	0.26270	1.00000
O26	4a	0.15030	-0.49870	0.35330	1.00000
O27	4a	-0.00510	-0.52890	0.28680	1.00000
O28	4a	0.08710	-0.52850	0.20000	1.00000
O29	4a	0.01980	0.14710	0.26130	1.00000
O30	4a	0.08540	-0.02690	0.19990	1.00000
O31	4a	0.17320	0.15910	0.29350	1.00000
O32	4a	0.11510	-0.03660	0.35260	1.00000

Table S4 The charge numbers of Mn ions for $LiZnPO_4:0.14Mn^{2+}$.

Sites	Original valence electrons	Remaining valence electrons	Transferring electrons
Mn1	7	5.6035	1.3965
Mn2	7	5.3900	1.61
Mn3	7	5.3722	1.6278

Table S5 The amounts of all the elements through ICP-OES analysis for $LiZnPO_4:0.14Mn^{2+}$.

Elements	Li	Zn	P	O	Mn
Theoretical wt%	4.2271	33.7560	18.7198	38.6473	4.6498
Experimental wt%	4.9189	33.9190	19.0444	37.3079	4.8098

Table S6 The total Helmholtz free energies for $LiZnPO_4+V_O$ and $LiZnPO_4:Mn^{2+}+V_O$.

Samples	defect state	formation energy
$LZP+V_O$	0	-666.26
	+1	-672.46
	+2	-676.89
$LZPM_{0.14}+V_O$	0	-688.65
	+1	-696.54
	+2	**-703.68**

Table S7 The defect formation energies without and with V_O for $LiZnPO_4:Mn^{2+}$.

Defect formation energy (eV)	$LiZnPO_4:Mn^{2+}$ (without V_O)	$LiZnPO_4:Mn^{2+}$ (with V_O)
Mn_{Zn}	-1.44	-2.66 (V_O)
		-2.89 ($V_O^{·}$)
		-3.13 ($V_O^{··}$)

Notes and references

1   B. Y. Qu, B. Zhang, L. Wang, R. L. Zhou and X. C. Zeng, *Chem. Mater.*, 2015, **27**, 2195-2202.

2   J. P. Perdew, W. T. Yang, K. Burke, Z. H. Yang, E. K. U. Gross, M. Scheffler, G. E. Scuseria, T. M. Henderson, I. Y. Zhang, A. Ruzsinszky, H. W. Peng, J. W. Sun, E. Trushin and A. Görling, *P. NATL. ACAD. SCI.*, 2017, **114**, 2801-2806.

3   Y. Nobuhiko, *J. Phys. Soc. Jpn.*, 1973, **35**, 1089-1097.